Application of the WRF-LETKF Data Assimilation System over Southern South America: Sensitivity to Model Physics

MARÍA E. DILLON,[*,+] YANINA GARCÍA SKABAR,[*,#] JUAN RUIZ,[@,#] EUGENIA KALNAY,[&] ESTELA A. COLLINI,[**,++] PABLO ECHEVARRÍA,[++] MARCOS SAUCEDO,[@,#] TAKEMASA MIYOSHI,[##] AND MASARU KUNII[&&]

[*] *CONICET, National Meteorological Service, Buenos Aires, Argentina*
[+] *Department of Atmospheric and Oceanic Science, Universidad de Buenos Aires, Buenos Aires, Argentina*
[#] *UMI-IFAECI, Buenos Aires, Argentina*
[@] *CIMA, CONICET, Department of Atmospheric and Oceanic Science, Universidad de Buenos Aires, Buenos Aires, Argentina*
[&] *Department of Atmospheric and Oceanic Science, University of Maryland, College Park, College Park, Maryland*
[**] *Naval Hydrographic Service, Buenos Aires, Argentina*
[++] *National Meteorological Service, Buenos Aires, Argentina*
[##] *RIKEN Advanced Institute for Computational Science, Kobe, Japan*
[&&] *Meteorological Research Institute, Tsukuba, Japan*

(Manuscript received 26 November 2014, in final form 14 August 2015)

ABSTRACT

Improving the initial conditions of short-range numerical weather prediction (NWP) models is one of the main goals of the meteorological community. Development of data assimilation and ensemble forecast systems is essential in any national weather service (NWS). In this sense, the local ensemble transform Kalman filter (LETKF) is a methodology that can satisfy both requirements in an efficient manner. The Weather Research and Forecasting (WRF) Model coupled with the LETKF, developed at the University of Maryland, College Park, have been implemented experimentally at the NWS of Argentina [Servicio Meteorológico Nacional (SMN)], but at a somewhat lower resolution (40 km) than the operational Global Forecast System (GFS) at that time (27 km). The purpose of this work is not to show that the system presented herein is better than the higher-resolution GFS, but that its performance is reasonably comparable, and to provide the basis for a continued improved development of an independent regional data assimilation and forecasting system. The WRF-LETKF system is tested during the spring of 2012, using the prepared or quality controlled data in Binary Universal Form for Representation of Meteorological Data (PREPBUFR) observations from the National Centers for Environmental Prediction (NCEP) and lateral boundary conditions from the GFS. To assess the effect of model error, a single-model LETKF system (LETKF-single) is compared with a multischeme implementation (LETKF-multi), which uses different boundary layer and cumulus convection schemes for the generation of the ensemble of forecasts. The performance of both experiments during the test period shows that the LETKF-multi usually outperforms the LETKF-single, evidencing the advantages of the use of the multischeme approach. Both data assimilation systems are slightly worse than the GFS in terms of the synoptic environment representation, as could be expected given their lower resolution. Results from a case study of a strong convective system suggest that the LETKF-multi improves the location of the most intense area of precipitation with respect to the LETKF-single, although both systems show an underestimation of the total accumulated precipitation. These preliminary results encourage continuing the development of an operational data assimilation system based on WRF-LETKF at the SMN.

1. Introduction

Forecast errors from numerical weather prediction (NWP) models arise in part from imperfect initial conditions, as a result of the lack of sufficient observations as

Corresponding author address: María E. Dillon, National Meteorological Service, 25 de Mayo 658 (C1002ABL), Buenos Aires, Argentina.
E- mail: mdillon@smn.gov.ar

DOI: 10.1175/WAF-D-14-00157.1

well as their suboptimal use. Different data assimilation systems (DASs) have been developed since the objective analysis of meteorological fields was introduced in the midtwentieth century; for example, Cressman (1959) developed the empirical successive corrections method and Gandin (1963) introduced optimal interpolation (the first statistical interpolation method). The complexity of the methodologies increased in step with the state-of-the-art computing resources.

Although there are now several methods in use, they all share a common use of a statistical combination of observations and short-range forecasts to calculate accurate initial conditions (Kalnay 2003). Currently most state-of-the-art data assimilation systems are based either on the variational or on the ensemble-based approaches, which adopt different ways for estimating the atmospheric state given from the information provided by the observations and the short-range forecast. Some of the strengths of ensemble-based data assimilation systems are that the evolution of the background error covariance from one assimilation window to the next can be estimated, and that these systems are also easier to implement than four-dimensional variational data assimilation (4DVAR) because the tangent linear and the adjoint of the numerical model are not required (Lorenc 2003; Kalnay et al. 2007; Meng and Zhang 2007). More recently, hybrid configurations between both DAS approaches have been proposed in order to combine their best features (e.g., Wang et al. 2008; Kleist 2012; Penny 2014; Hamrud et al. 2014).

Relatively few data assimilation studies have been focused on the impact of data assimilation over southern South America. Among the experiments with real observations, García Skabar and Nicolini (2009) used observations from the South American Low-Level Jet Experiment (SALLJEX; Vera et al. 2006) to generate enriched analyses through nudging. In Brazil the Centro de Previsão de Tempo e Estudos Climáticos (CPTEC) runs the Regional and Global Physical-Space Statistical Analysis System (da Silva et al. 1995; Herdies et al. 2002, 2007), and more recently they have carried out studies with a global three-dimensional variational data assimilation (3DVAR) system based on the Gridpoint Statistical Interpolation analysis system (GSI; Azevedo and de Goncalves 2015; de Goncalves and Azevedo 2015). Furthermore, Saucedo et al. (2014) performed observing system simulation experiments (OSSEs) over South America using the Weather Research and Forecasting (WRF) Model–local ensemble transform Kalman filter (WRF-LETKF) DAS, in order to evaluate the impact of different error sources on the accuracy of the regional analysis system.

The development and implementation of an operational data assimilation scheme as well as an ensemble forecast configuration for an NWP model is considered essential for any major national weather service (NWS). For instance, the meteorological offices of the United States [National Centers for Environmental Prediction (NCEP)], the United Kingdom [Met Office (UKMO)], Canada [Canadian Meteorological Centre (CMC)], Japan [Japan Meteorological Agency (JMA)], Europe [European Centre for Medium-Range Weather Forecasts (ECMWF)], and Brazil (CPTEC) are running different ensemble forecasting systems, both global and regional. Some of them have already implemented a hybrid DA configuration (Met Office, NCEP, and ECMWF), merging variational and ensemble methods to obtain the analyses, while others run variational DAS first and then calculate ensemble perturbations (JMA and CPTEC).

Ensemble-based data assimilation systems are an appealing choice since they can provide a state-of-the-art data assimilation system as well as initial conditions for ensemble forecasts. Moreover, the ensemble Kalman filter (EnKF) is essentially independent of the model, and computationally efficient with tunable parameters such as the localization and the inflation, which enable some flexibility depending on the scale of the problem. This methodology is currently used operationally in CMC through an ensemble variational (EnVar) DAS (Houtekamer et al. 2014; Buehner and Shlyaeva 2015), and this is the first case in which 4DVAR has been replaced with a more advanced ensemble-based method.

In the ensemble-based systems, the forecast uncertainty is estimated directly from an ensemble of forecasts. If each ensemble member is produced by the same model equations, then the ensemble spread cannot represent the forecast errors associated with model errors (Houtekamer et al. 1996). Meng and Zhang (2007) summarized the different approaches for including model error in ensemble forecasts such as the use of different forecast models, the use of different physical parameterization schemes, the application of statistical adjustments, the inclusion of adaptive multiplicative inflation, the use of an additive inflation method, and the use of a covariance relaxation method, among others.

The multischeme approach is a simple way to take into account model uncertainties associated with parameterization of the unresolved processes, which is one of the main sources of model error in current NWP models (Stensrud et al. 2000). Currently, the NCEP Short-Range Ensemble Forecast (SREF) system runs with 21 members of multi-analysis, multimodel, and multiphysics configurations, providing useful and critical information to forecasters across the North American domain (Du et al. 2014).

Moreover, additional spread provided by the multischeme approach is state dependent (e.g., additional ensemble spread will be larger in areas where a particular parameterization is active, for example, over a heavy

convective rain situation). In addition, multischeme ensembles tend to have lower biases than ensembles that use one single model and thus, in this sense, this approach is more consistent with assumptions made in data assimilation schemes. Over North America, Meng and Zhang (2007) showed that using a combination of different cumulus parameterization schemes improves the performance of the EnKF: this experiment had a smaller bias and a better background error covariance structure than the single scheme. They also found that including model uncertainties from planetary boundary layer (PBL) and microphysical processes had significant impacts on the EnKF skill. Similar results were achieved over South America by M. Saucedo (2015, unpublished manuscript) who found that the inclusion of a physical ensemble (using a combination of cumulus, PBL, and microphysics parameterizations) within an idealized framework using the LETKF has a positive effect in terms of analysis quality, reducing both the systematic and nonsystematic errors.

Our long-term goal is to develop a regional numerical weather prediction (RNWP) system for the NWS of Argentina [Servicio Meteorológico Nacional (SMN)] capable of producing forecasts that should be complementary with the advanced, higher-resolution, and very mature NCEP Global Forecast System (GFS) forecasts, generously available on the Internet for operational use. Within this context, this paper shows the results of the first step, namely the development and testing of a regional data assimilation/forecasting system based on the WRF-LETKF DAS originally developed by Miyoshi and Kunii (2011). At this stage, we are using a relatively coarse resolution in order to test the system, while as a next step we plan to use a higher-resolution model where local observations such as radar data could also be included. The RNWP system that we are testing here will also provide evolving ensemble boundary conditions for a nested higher-resolution DAS.

The main purpose of this work is to compare two possible implementations of the regional data assimilation system based on the single-model and multischeme approaches, and to provide a first evaluation of the regional DAS, showing that its performance is reasonably comparable to the mature and higher-resolution GFS routinely produced by NCEP. To accomplish this, the system is tested using real observations during the spring of 2012.

This paper, which provides the basis for the continuing development of an independent regional data assimilation and forecasting system, is organized as follows. Section 2 describes the details of the implementation of the data assimilation system and the different experiment configurations. An evaluation of its performance and the impact of using the multischeme ensemble are presented in section 3, along with an analysis of an intense precipitation case study. Finally, concluding remarks are presented in section 4.

2. Data and methodology

a. Experimental design

To accomplish our objective, we use the WRF-LETKF DAS developed at the University of Maryland, College Park (Hunt et al. 2007; Miyoshi and Kunii 2011), which is open source (http://code.google.com/p/miyoshi/) and has been tested in different experiments (Miyoshi et al. 2007; Yang et al. 2009; Seko et al. 2011; Miyoshi and Kunii 2012; Saucedo et al. 2014). In our region, the Advanced Research version of WRF (Michalakes et al. 2004; Skamarock et al. 2008) has been adopted in research (Saulo et al. 2008; Ruiz et al. 2010; Dillon et al. 2013) as well as in experimental operational usages.

The selected domain covers central and southern South America (Fig. 1) using a Lambert projection and a relatively coarse grid size of 40 km (139 × 134 grid points), representing a regional–synoptic-resolution domain adequate for a first evaluation of this DAS over South America. For the vertical, 30 sigma-p levels are used with the model top at 50 hPa. A 2-month test period is selected during the Southern Hemisphere spring, from 1 November to 31 December 2012, when the Cloud Processes of the Main Precipitation Systems in Brazil: A Contribution to Cloud-Resolving Modeling and to the Global Precipitation Measurement (GPM) field campaign, performed over Santa Maria (in Brazil) (CHUVA-SUL; Machado et al. 2013), took place, and during which some intense convective systems developed over the region.

The ensemble size in the experiments is 40. For the generation of the initial conditions at 0000 UTC 1 November 2012, 40 perturbations across the entire atmospheric state are generated and added to the GFS deterministic analysis. These perturbations are calculated as differences between 24-h consecutive atmospheric states, starting at 0000 UTC 15 October and ending at 0000 UTC 24 November 2010. These differences are scaled by a constant factor of 0.2. Perturbations generated in this way are balanced, thus increasing their chance of projecting onto the unstable modes of the system and reducing the convergence time of the forecast error covariance matrix.

For the boundary conditions, all of the ensemble members use the same deterministic GFS forecasts initialized at the analysis time, following the results of Miyoshi and Kunii (2011). Since including perturbations at the lateral boundary ameliorates the underestimation of the ensemble spread and improves the analyses (Zhang et al. 2004; Saito et al. 2012; Saucedo et al. 2014), we consider the inclusion of perturbations at the boundaries to be a priority in future improvements to the system. An

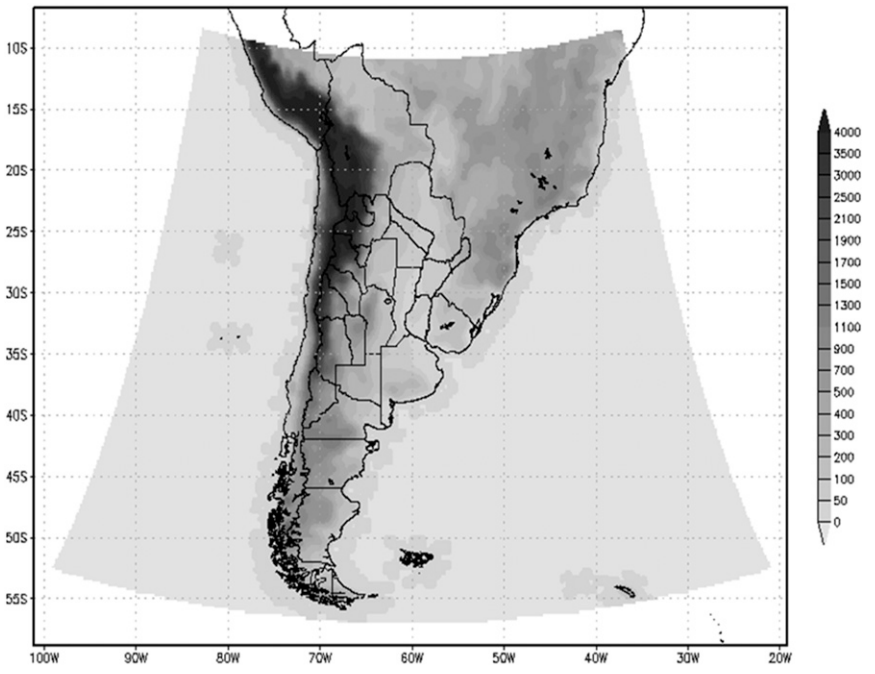

FIG. 1. Model domain and topography (m MSL; shaded).

advantage of using the GFS forecasts as boundary conditions is that our experiments will be indirectly influenced, through its boundaries, by the observations assimilated by the global model, especially by satellite radiances, which have been demonstrated to be very important in reducing the short-range forecast errors (e.g., Ota et al. 2013).

Two data assimilation experiments are performed. In the first experiment, all of the ensemble members use the same model configuration: Kain–Fritsch for cumulus (Kain 2004), WSM6 for microphysics (Hong and Lim 2006), Yonsei University (YSU) for the planetary boundary layer (Hong Noh and Dudhia 2006), RRTM for longwave radiation (Mlawer et al. 1997), Dudhia for shortwave radiation (Dudhia 1989), and the Noah land surface model (Chen and Dudhia 2001). The selection of these options corresponds to previous results carried out over South America (Ruiz et al. 2010; Saulo et al. 2008), although we are aware that it is not possible to choose the "best" parameterization configuration as the performance depends on different factors, such as the region, the season, the variable or variables considered in the verification, and the synoptic environment, among others. This single-model experiment will be referred to as LETKF-single.

In the second experiment, a multischeme approach is implemented inspired by the promising results obtained with this technique by several authors (e.g., Stensrud et al. 2000; Meng and Zhang 2007; Saucedo et al. 2014) and will be referred to as LETKF-multi. Nine different combinations of cumulus and PBL schemes are used, as described in Table 1, which also shows the number of ensemble members that use each combination. All other model settings and parameterizations remained equal to the LETKF-single run. One drawback of a multischeme approach is that the ensemble members are not equally probable. Usually, different configurations have different forecast skills and none of them produces the best result for all the variables over the entire domain. In this sense, the allocation of specific weights to each member would be inappropriate unless a statistic experiment is carried out beforehand.

Observations are assimilated in 3-h windows using a 4D-LETKF approach (Miyoshi and Kunii 2011) providing us with initial conditions every 3 h. The assimilation window starts 3 h before the analysis time and ends at the analysis time (Fig. 2). Within the assimilation window, observations are grouped in hourly time slots. Using a data assimilation window that ends at the analysis time, the analysis can be obtained earlier. Another advantage of this implementation is that initial conditions for forecast initialization are available at a higher frequency than those provided by NCEP GDAS, which are currently available every 6 h, and which might be particularly useful in situations favorable for the occurrence of extreme weather events. In addition, this higher assimilation frequency would allow for a future implementation of the "no-cost smoother" proposed by Kalnay and Yang (2010), as it meets the conditions needed of a short assimilation window. One drawback of

TABLE 1. Different model configurations used in LETKF-multi. An uppercase letter is used to identify each particular configuration. The number of ensemble members for each configuration is provided in parentheses.

		Cumulus scheme		
		Kain–Fritsch (Kain 2004)	BMJ (Janjic 1994)	Grell (Grell and Devenyi 2002)
PBL scheme	YSU (Hong Noh and Dudhia 2006)	A (five members)	B (five members)	C (five members)
	MYJ (Janjic 2002)	D (five members)	E (four members)	F (four members)
	Quasinormal (Sukoriansky et al. 2005)	G (four members)	H (four members)	I (four members)

our implementation is that the assimilation window is not centered on the analysis time, thus potentially producing a degradation in the analysis quality since the observations are not assimilated as close as possible to the time of the analysis. The impact of this approach will be explored in future studies.

One of the most important parameters in LETKF is the forecast error covariance localization scale. In this work, a value of 400 km is used for the horizontal localization, and a value of 0.4 ln$p$ is selected as the vertical localization scale (~4 km) (Miyoshi et al. 2007, 2010; Miyoshi and Kunii 2011). Another important parameter is the multiplicative inflation, whose role is to prevent underestimation of the forecast error covariance leading to filter divergence (Anderson and Anderson 1999). In this work, the adaptive inflation technique developed by Miyoshi (2011) and implemented within WRF-LETKF by Miyoshi and Kunii (2012) is used. This method allows an online estimation of a location and time-dependent optimal inflation factor based on the innovation statistics.

The adaptive multiplicative inflation factor has a rather long spinup time, so in this paper, a first data assimilation experiment was run for 2 months in order to spin up this factor. The inflation values obtained at the end of this experiment are used as initial values for the experiments that will be presented in the results section. Figure 3 shows the time evolution of the spatially averaged inflation factor for the LETKF-multi experiment, for 850 and 500 hPa. As expected, the adaptive inflation is larger during the times with more observations (0000 and 1200 UTC; see Fig. 5, described in greater detail below), and is also larger at 850 than at 500 hPa since the former is influenced by surface observations. The change of slope after 2 months corresponds to the reinitialization of the data assimilation experiment. This change probably responds to the difference in the initial values of the estimated multiplicative inflation when the experiment is reinitialized: as the second data assimilation cycle starts with higher inflation values, the ensemble spread is larger from the beginning, and the adaptive inflation values do not increase as fast as in the first cycle. The experiments carried out by Miyoshi and Kunii (2012) showed a convergence time of the estimated inflation parameter of around 4 months using real observations. However, this might be dependent on the number of available observations (Miyoshi 2011).

Comparing the behavior of this parameter between the LETKF-single and LETKF-multi experiments during the second assimilation cycle, it is found that the average inflation values over all model grid points and levels in the LETKF-multi experiment are 0.037 and 0.07 lower than in the LETKF-single experiment, for 0000 and 1200 UTC, respectively. It is expected that we will find less values of this parameter in LETKF-multi because the multischeme configuration provides an error source, somehow lightening the inflation job. However, for the other analysis cycles (0300, 0600, 0900, 1500, 1800, and 2100 UTC) the inflation factor of LETKF-multi is on average higher than the inflation factor of the LETKF-single run (between 0.008 and 0.048). Nevertheless, the magnitudes of these values are two orders less than the average inflation factors, indicating a very small difference between the experiments that is probably due to the limited amount of observations assimilated (see Fig. 5, described in greater detail below).

The vertically averaged inflation parameter field corresponding to the cycles of 0000 and 1200 UTC is presented in Fig. 4. The maximum values are located over the Atlantic Ocean, where satellite-derived wind

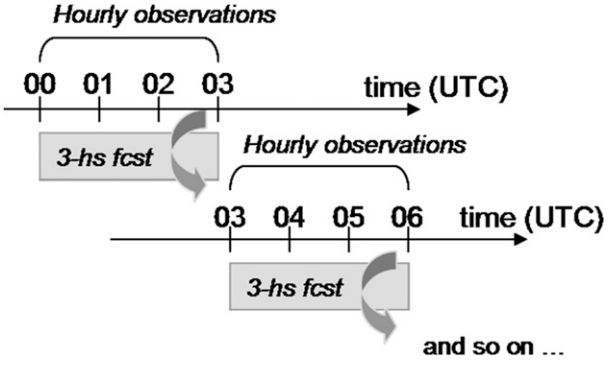

FIG. 2. Assimilation cycle scheme.

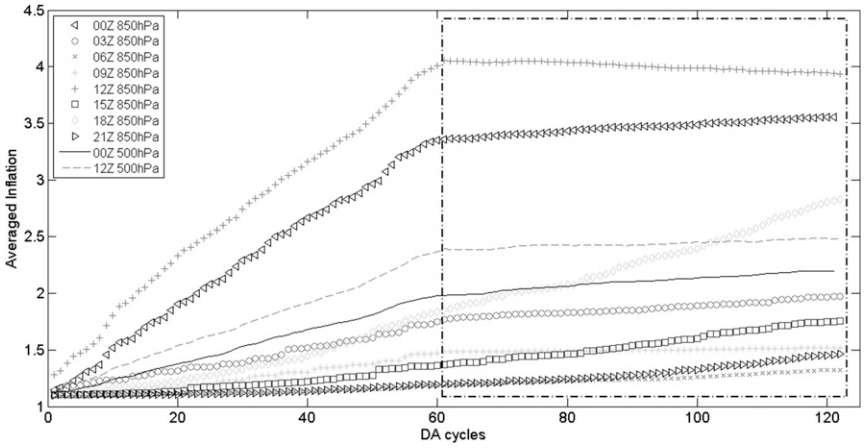

FIG. 3. Spatially averaged inflation as a function of the assimilation cycle, for LETKF-multi, for all the analysis hours at 850 hPa, and for 0000 and 1200 UTC at 500 hPa. The dot–dashed square represents the period effectively used for the results presented in this work (see text for details).

observations are denser and close to the area where upper-air observations are denser.

b. Observations

For these experiments real observations from the prepared data in Binary Universal Form for Representation of Meteorological Data (PREPBUFR) files generated at NCEP are used (Keyser 2013). The observations available in our region are from ships, aircrafts, surface stations, and radiosondes, as well as satellite estimations of atmospheric motion vectors (AMVs) calculated from the Geostationary Operational Environmental Satellite (GOES) and near-surface wind vector fields derived from the Advanced Scatterometer

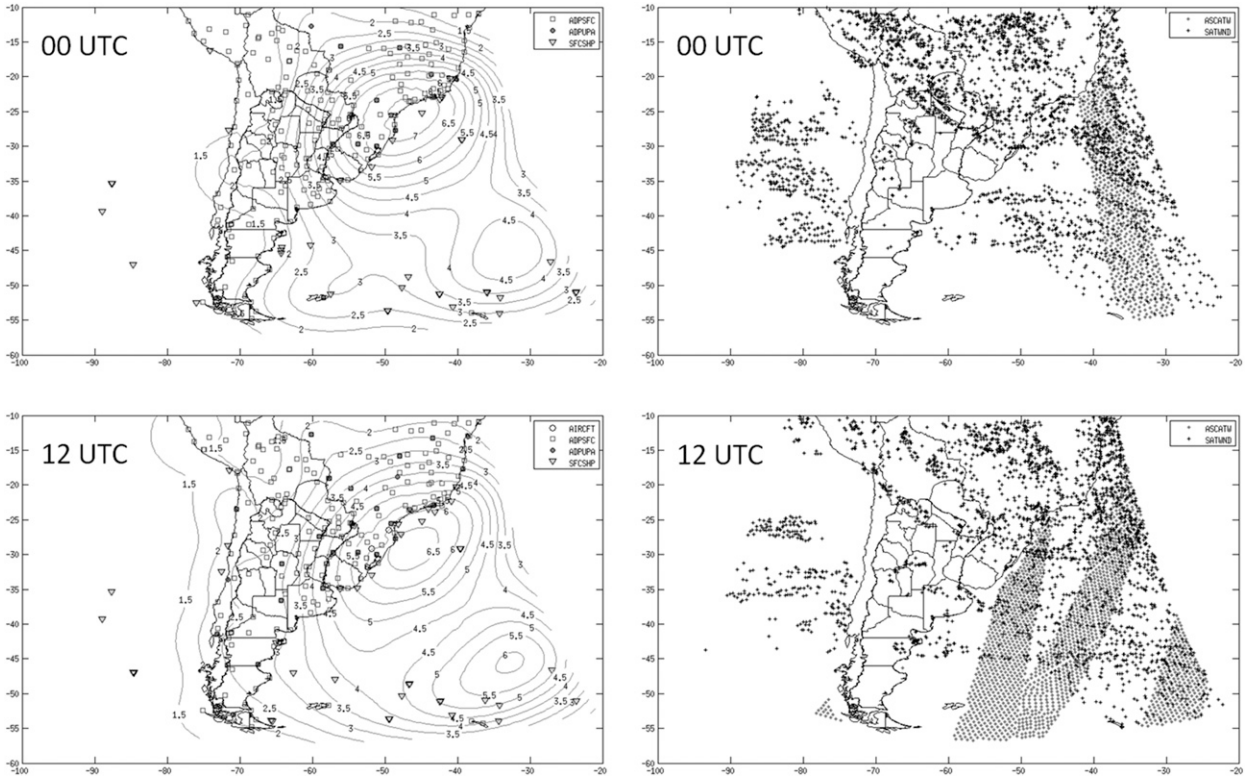

FIG. 4. Types of data assimilated at (top) 0000 and (bottom) 1200 UTC 31 Dec 2012. The mean inflation parameter for each cycle (contours) is also shown in (left).

(ASCAT; Verspeek et al. 2009). To illustrate the spatial distribution for the different observation types, an example of the observations assimilated during the analyses cycles at 0000 and 1200 UTC 31 December is shown in Fig. 4.

The spatial resolution of the GOES AMVs is not fixed because its calculation depends on the instantaneous clouds pattern, while the horizontal resolution of the sea surface winds from ASCAT is always about 0.25°. To reduce the error covariance among ASCAT observations, which is not well known and not accounted for in the current implementation of the filter, the data have been interpolated onto a 0.5° × 0.5° grid using a box-averaging technique (Pauley et al. 2012). An error of $2\,\mathrm{m\,s^{-1}}$ is assumed for this observation type according to NASA's Physical Oceanography Distributed Active Archive Center.

Figure 5 summarizes the quantity of available observations for each cycle, showing the mean number of assimilated observations over the 61 days of the experiments. With respect to the wind observations, the GOES AMVs only contribute in the principal cycles because of the configuration of the PREPBUFR files, where these data are available only 1 h prior to their analysis time (i.e., 0500, 1100, 1700, and 2300 UTC). ASCAT's surface winds availability depends on the satellite schedule, and this leads to a lack of information at 0900 and 2100 UTC in our region. There is a lack of thermodynamic observations during most of the eight analysis cycles, because of the small number of radiosondes that mostly correspond to the cycles of 0000 and 1200 UTC.

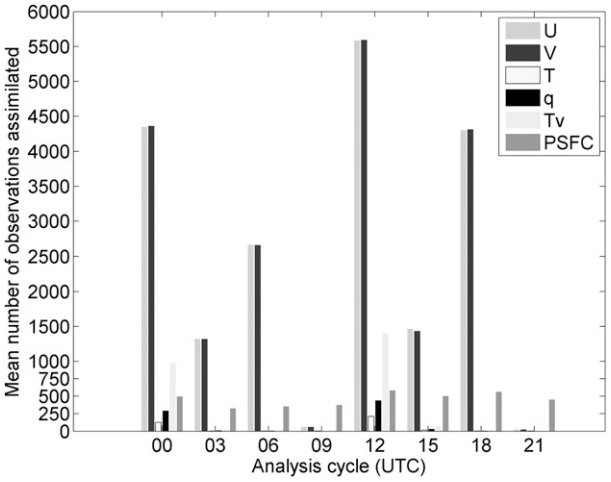

FIG. 5. Mean number of observations assimilated: u, v, temperature T, q, T_v, and surface pressure (PSFC), for all of the analysis hours.

c. *Verification methods*

To evaluate the analysis quality, the bias and the root-mean-square difference (RMSD) scores for the entire period were calculated, considering both the differences between the observations O and the analyses A ($O - A$), and between the observations and the forecasts F ($O - F$), using radiosondes. The GFS analyses and forecasts are included in this evaluation, and their statistics are compared with those of our experiments. We selected GFS as a benchmark because it constitutes a mature state-of-the-art global data assimilation and forecasting system that incorporates many different data sources (i.e., the conventional observations that we used as well as many satellite radiances).

For the selected case study, a verification of forecasted accumulated precipitation was also performed. The Tropical Rainfall Measuring Mission (TRMM) Multisatellite Precipitation Analysis (TMPA) 3B42-V7 algorithm (Huffman et al. 2007; Huffman and Bolvin 2013), with a spatial resolution of 0.25° and a temporal resolution of 3 h, is used as verifying truth because it was found to provide an acceptable representation of precipitation over our region (Salio et al. 2014) and because it has greater spatial and temporal resolutions than the available rain gauge network.

For determining their performance statistically the bias score (BIASS), equitable threat score (ETS), probability of detection (POD), and false alarm rate (FAR) are calculated for precipitation thresholds ranging from 0.5 to 20 mm $(3\,\mathrm{h})^{-1}$, during the 12-h period of most intense precipitation. The value obtained with a perfect forecast for ETS and POD is 1, while for FAR it is 0. Overestimation (underestimation) is described by BIASS greater (lower) than 1. Although these scores can be affected by the bias of the precipitation data of TMPA, this is smaller than the bias of the models, and therefore TMPA is still a very useful tool (Salio et al. 2014).

The probability distribution function (PDF) of accumulated precipitation (Amitai et al. 2011) is determined for the experiments, in order to consider the relative contribution of each precipitation interval to the total precipitation volume. The volumetric PDF is defined as the sum of the rain rates for a given 1-dBR interval (dBR = $10\log\{R/[1\,\mathrm{mm}\ (3\,\mathrm{h})^{-1}]\}$; R [mm $(3\,\mathrm{h})^{-1}$]) divided by the total sum of the rain rates:

$$\mathrm{PDF}(R_i) = \frac{\int_{R_i-0.5}^{R_i+0.5} RP(R)\,dR}{\int_0^{\infty} RP(R)\,dR}, \qquad (1)$$

where R represents the amount of rainfall, $P(R)$ represents the probability of rain-rate occurrence, and i is the 1-dBR interval bin number. This distribution is

calculated for each experiment and for the TMPA estimate, considering the 12-h period of most intense precipitation over a specific rectangular region that will be defined later. This kind of measure represents a global comparison among the different precipitation distributions and, therefore, is complementary to the evaluation given by ETS, POD, FAR, and BIASS.

3. Results

a. *Verification of the quality of the analysis and short-range forecasts over the entire experimental period*

To examine the performance of LETKF-single and LETKF-multi, the bias and RMSD between the observations and each ensemble mean were calculated. Vertical profiles of bias and RMSD were computed at 1200 UTC using radiosonde observations from 23 stations at 975, 925, 900, 850, 800, 700, 600, 500, 400, 300, and 250 hPa (1200 UTC is selected because the number of radiosonde observations is higher at this time). The variables evaluated are the zonal u and meridional v wind components, virtual temperature T_v, and specific humidity q. The numbers of total observations used for the verification at each level are summarized in Table 2. These radiosondes were already assimilated into the WRF-LETKF experiments and into GFS, and consequently they are not independent of the 1200 UTC analyses. When they are used in the forecasts evaluations, the radiosondes are independent because they were not known at 0600 UTC (the corresponding analysis time).

TABLE 2. Number of observations at each vertical level and for different variables, used for the verification.

Vertical level (hPa)	u	v	T_v	q
250	1198	1198	—	—
300	1200	1200	1190	870
400	1203	1203	1200	1043
500	1203	1202	1200	1082
600	1066	1065	832	761
700	1199	1200	1195	1153
800	1054	1054	664	643
850	1200	1200	1192	1185
900	1056	1054	744	738
925	988	986	969	970
975	663	662	266	266

Figure 6 shows the results for the 1200 UTC analyses. Generally, the structure of the RMSD is similar for the different DAS. LETKF-multi presents a lower RMSD than LETKF-single for u and v, while for the specific humidity LETKF-multi RMSD is lower below 800 hPa. No substantial difference is found between the two experiments for the virtual temperature. With respect to the bias, for the wind components LETKF-multi shows a slightly lower result than LETKF-single. However, for T_v and q LETKF-single generally presents lower bias than LETKF-multi. GFS analyses show a smaller RMSE and bias for most vertical levels and variables when compared with the WRF-LETKF experiments.

For a more independent evaluation, the bias and RMSD for the 6-h forecast that verifies at 1200 UTC have been computed. Figure 7 shows that the RMSDs of LETKF-multi forecasts are usually less than the ones of LETKF-single for u, v, and q, while for T_v both experiments have roughly the same values. Regarding the bias, LETKF-multi shows better performance than LETKF-single for u and q at low levels, and for v over the entire vertical column. These statistics were also calculated for the 3-h forecasts of both LETKF experiments (i.e., forecasts initialized with the 0900 UTC analyses), and similar results were found: LETKF-multi generally presents improvements with respect to LETKF-single (not shown).

These results are in accordance with the fact that multischeme ensembles tend to have lower biases than ensembles that use a single model (Meng and Zhang 2007; Saucedo et al. 2014). Moreover, the magnitude of the errors found in this work is similar to what Miyoshi and Kunii (2011) showed in their study with real observations over the western Pacific.

GFS forecasts show a better performance than the WRF forecasts initialized from the WRF-LETKF experiments (Fig. 7). Although it is clear that the GFS outperforms both experiments, at least at this development stage, the results suggest that the proposed data assimilation system does a reasonable job, particularly if we take into account that GFS runs at a higher horizontal resolution with respect to our DAS (27 vs 40 km) and also incorporates radiances from many satellites not used in the LETKF-WRF experiments, especially since the assimilation of radiances is very important over regions with limited availability of conventional observations, and therefore it has a large impact over the Southern Hemisphere (Kalnay 2003). Many authors have shown positive results by assimilating radiances from different sensors and over distinct areas (e.g., Köpken et al. 2004; McCarty et al. 2009; Schwartz et al. 2012; Xu et al. 2013). In this sense, better results of our DAS could be attained through the incorporation of either satellite radiances and/or retrievals of temperature and humidity profiles in the assimilation, since the radiosonde observations are spatially and temporally much sparser (Figs. 4 and 5). Including these types of observations and more

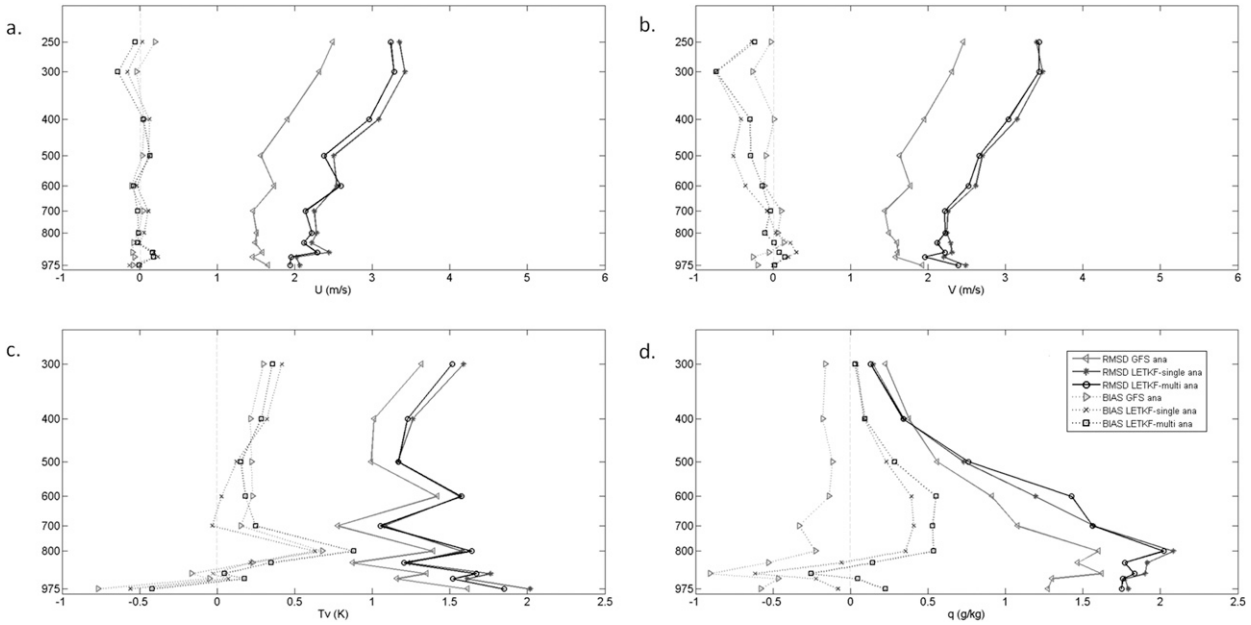

FIG. 6. Bias and RMSD calculated for the 1200 UTC analyses of GFS, and the ensemble means of LETKF-single and LETKF-multi, relative to radiosondes observations, for (a) u ($\mathrm{m\,s^{-1}}$), (b) v ($\mathrm{m\,s^{-1}}$), (c) T_v (K), and (d) q ($\mathrm{g\,kg^{-1}}$).

frequent GOES AMVs input (the National Oceanic and Atmospheric Administration actually provides 3-hourly products) is planned in order to improve our results and to try and solve the problems that we have found concerning the lack of observations (especially at 0900 and 2100 UTC).

One inherent issue with regional DAS and forecasting systems is that the presence of boundaries may negatively affect the performance of these systems with respect to global systems, even at a similar horizontal resolution, through the propagation of boundary errors onto the interior of the domain. For more insight, please

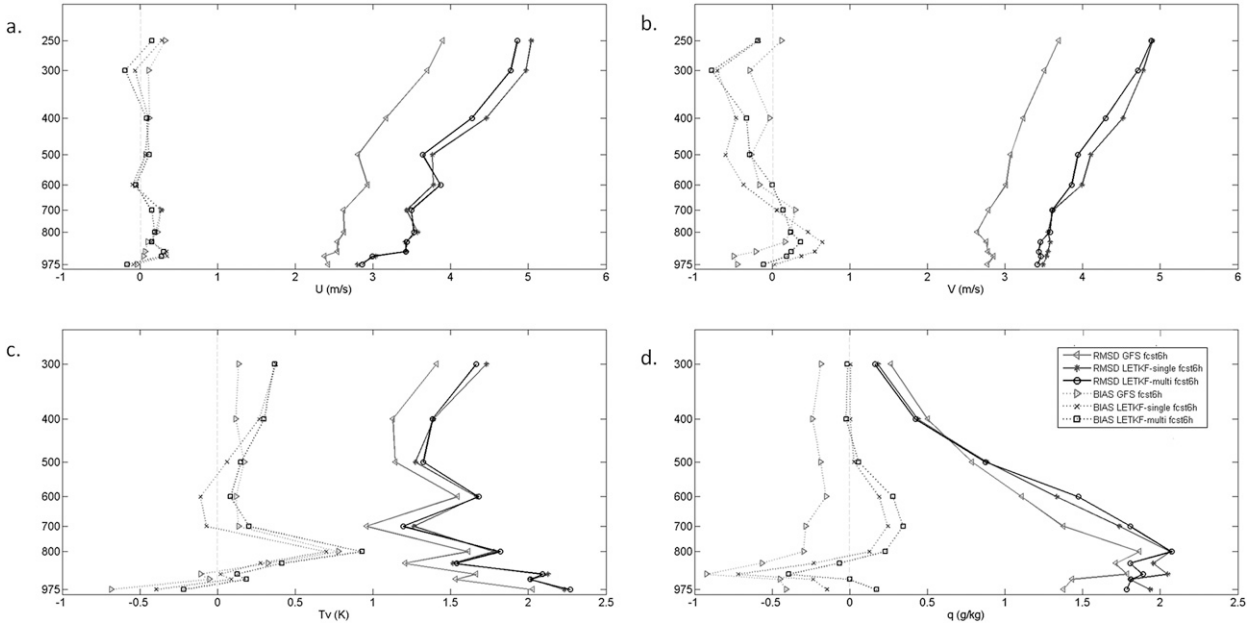

FIG. 7. Bias and RMSD calculated for the 1200 UTC 6-h forecasts of GFS, and the ensemble means of LETKF-single and LETKF-multi, relative to radiosondes observations, for (a) u ($\mathrm{m\,s^{-1}}$), (b) v ($\mathrm{m\,s^{-1}}$), (c) T_v (K), and (d) q ($\mathrm{g\,kg^{-1}}$).

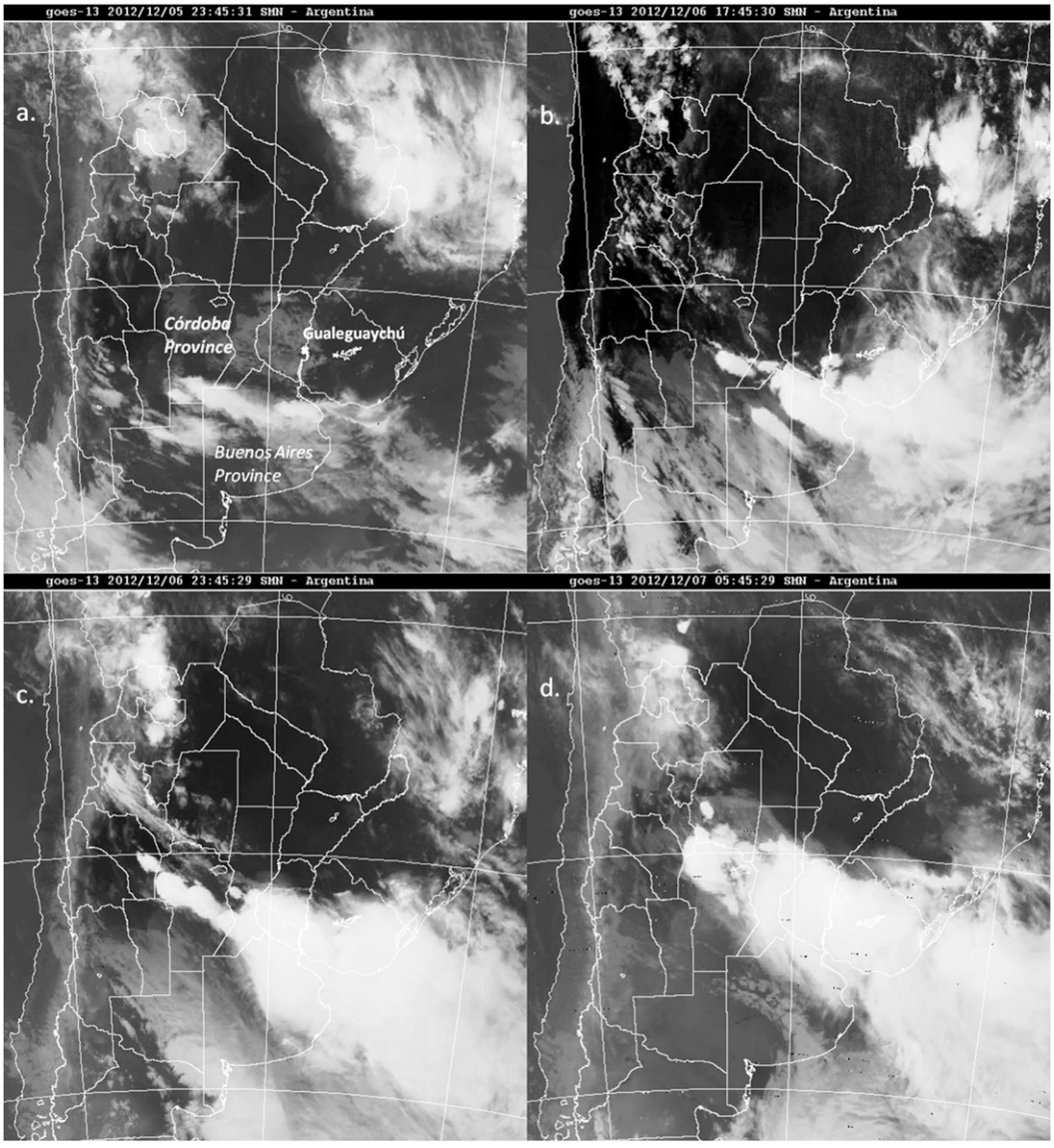

FIG. 8. Infrared images from *GOES-13* at (a) 2345 UTC 5 Dec, (b) 1745 UTC 6 Dec, (c) 2345 UTC 6 Dec, and (d) 0545 UTC 7 Dec. (Figures provided by SMN.) The locations of the city Gualeguaychú and the provinces Córdoba and Buenos Aires are also shown.

refer to Warner et al. (1997), who presented a very exhaustive and interesting research into the various types of lateral boundary conditions formulations and the corresponding recommendations for how their effects can be minimized. However, Wang et al. (2012) showed that the skill advantages of regional models compared with global systems might depend on the chosen variable and/or the vertical level considered.

b. A case study

For a preliminary evaluation of short-range ensemble forecasts produced by the different DAS compared in this work, the mesoscale convective system (MCS) that took place over central and eastern Argentina between 6 and 7 December 2012 has been selected. These types of MCSs are quite frequent over our region, accounting for more than half of the observed warm season precipitation. This MCS developed in response to the combination of a slowly advancing cold front and the presence of the South American low-level jet (Salio et al. 2007) that favors moisture advection from subtropical latitudes into northern and central Argentina. Figure 8 summarizes the evolution of the system from its genesis during the night of 5 December, and up to the

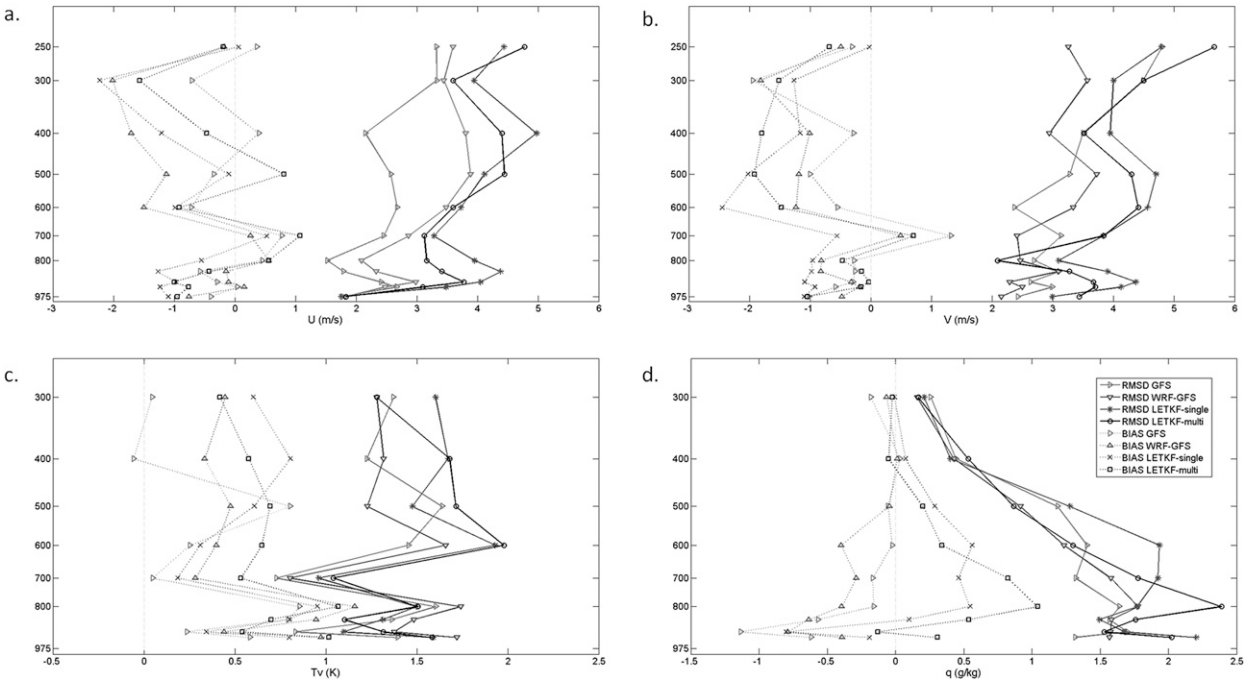

FIG. 9. Bias and RMSD for the 12-h forecasts (valid at 1200 UTC 6 Dec) from GFS, WRF-GFS, and the experiments initialized with the analysis ensemble mean of LETKF-single and LETKF-multi, relative to radiosonde observations, for (a) u ($\mathrm{m\,s^{-1}}$), (b) v ($\mathrm{m\,s^{-1}}$), (c) T_v (K), and (d) q ($\mathrm{g\,kg^{-1}}$).

beginning of its decaying stage in the early morning of 7 December. This convective system produced a huge amount of accumulated precipitation over certain regions; in addition, surface wind gusts that ranged from 17 to 36 $\mathrm{m\,s^{-1}}$ were reported at many surface stations in the province of Córdoba, and at least one tornado was reported in the city of Gualeguaychú.

The experiments carried out for this case consist of 48-h WRF forecasts initialized at 0000 UTC 6 December, using the GFS 3-hourly outputs for lateral boundary conditions. For each DAS experiment (LETKF-single and LETKF-multi), 41 forecasts were computed (40 forecasts initialized from the individual analysis ensemble members, and 1 forecast initialized from the analysis ensemble mean). A single run was also performed with WRF using the 0000 UTC 6 December GFS analysis as the initial conditions (WRF-GFS) and using the same model configuration of LETKF-single. In addition, the GFS forecasts are also verified and included in the comparison.

Figure 9 shows the bias and RMSD calculated for the 12-h forecasts of the experiments initialized with the analysis ensemble mean of LETKF-multi and LETKF-single, and of WRF-GFS and GFS single runs, with respect to the 1200 UTC 6 December radiosondes observations, in order to evaluate their performance for the case study. For the wind components, the RMSD for LETKF-multi is generally lower than that for LETKF-single while the difference in RMSD between both experiments is not so clear for the virtual temperature and specific humidity. LETKF-multi also shows lower bias for u and v at most vertical levels, but the difference between these experiments is not clear for the virtual temperature and the specific humidity.

The GFS forecast is the one that overall shows the best performance, followed by WRF-GFS. This is more clearly seen for u. The fact that WRF-GFS performs worse than GFS in this case study may be reflecting the lower resolution used in WRF-GFS and the impact of additional noise introduced at the boundaries of the regional domain, as well as differences in the model physics between WRF and GFS. All of these factors also affect the regional DAS, explaining the lower skill in the analysis and the short-range forecast discussed in the previous section.

With respect to the wind gusts registered by various surface stations throughout the province of Córdoba between 2300 UTC 6 December and 0400 UTC 7 December, the variable ''gustsfc'' from the common NCEP postprocessing program (Unipost) is analyzed. This variable estimates the gustiness and is calculated from the wind speed excess over the surface speed at each level within the PBL depth, and subsequently the maximum weighted wind excess is added

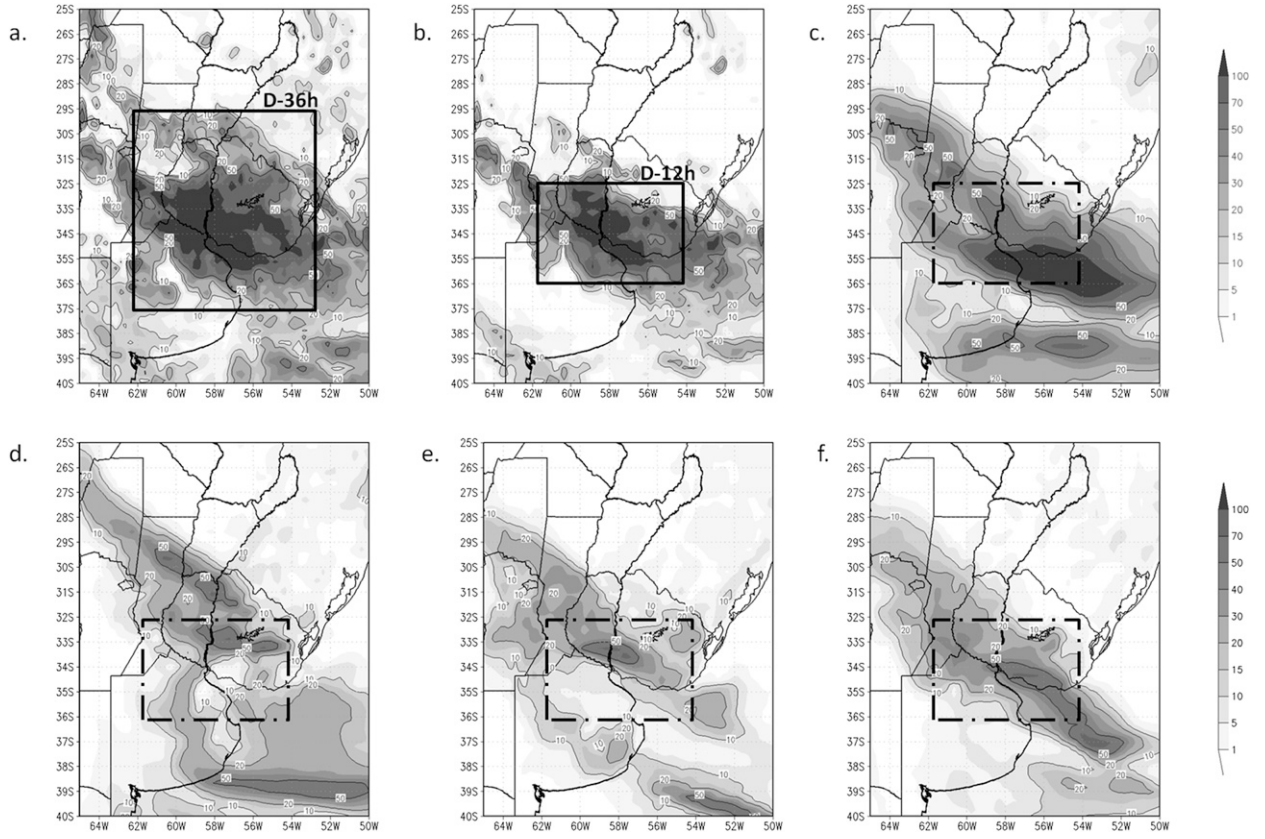

FIG. 10. Accumulated precipitation (mm) from TMPA estimates from (a) 0600 UTC 6 Dec to 1800 UTC 7 Dec and (b) 1800 UTC 6 Dec to 0600 UTC 7 Dec. Accumulated precipitation from 1800 UTC 6 Dec to 0600 UTC 7 Dec from (c) GFS, (d) WRF-GFS, (e) experiment initialized with the analysis ensemble mean of LETKF-single, and (f) experiment initialized with the analysis ensemble mean of LETKF-multi. Contours of 10, 20, and 50 mm are also displayed. The black boxes represent the domains D-36h (29°–37°S and 62°–53°W) and D-12h (32°–36°S and 62°–54°W) used in the computation of the verification scores and the PDF (see text for details).

back to the surface wind (for more details please refer to http://ruc.noaa.gov/rr/RAP_var_diagnosis.html#gust). Each experiment (LETKF-multi, LETKF-single, and WRF-GFS) shows a maximum in surface wind gusts during those hours but LETKF-multi reaches the largest value, which is 15 m s^{-1} (not shown). Although this is less than the values registered at the surface weather stations, which ranged from 17 to 36 m s^{-1}, the result is reasonable considering the horizontal resolution of the WRF Model (40 km). Regarding the GFS forecasts, the maximum in surface wind gust reached is slightly higher than in the LETKF experiments (18 m s^{-1}), but still less than the greatest value registered.

Finally, we evaluate the skill of the quantitative precipitation forecast for the four model runs. Figure 10 shows the 36-h accumulated precipitation between 0600 UTC 6 December and 1800 UTC 7 December (Fig. 10a) and the 12-h accumulated precipitation between 1800 UTC 6 December and 0600 UTC 7 December (Fig. 10b), according to the TMPA. The last was the most intense period of precipitation, and therefore the accumulated precipitation forecasted for those hours is shown for GFS (Fig. 10c), WRF-GFS (Fig. 10d), LETKF-single (run initialized with the analysis ensemble mean; Fig. 10e), and LETKF-multi (run initialized with the analysis ensemble mean; Fig. 10f).

All but the GFS forecast underestimate the largest accumulated precipitation values with respect to the TMPA data. This result again is probably a consequence of the limitations associated with the lower resolution and noise generated at the boundary that affects the forecast produced with WRF in these experiments. However, the area of maximum precipitation forecasted by the GFS is displaced to the southeast with respect to the observations, and it overestimates the precipitation over the southern part of the domain, particularly over the ocean.

As can be seen in Fig. 10, the LETKF-single and LETKF-multi experiments have better performance compared to WRF-GFS, mainly because in the latter there is a displacement of the precipitation area to the north with respect to TMPA. The spatial distribution of

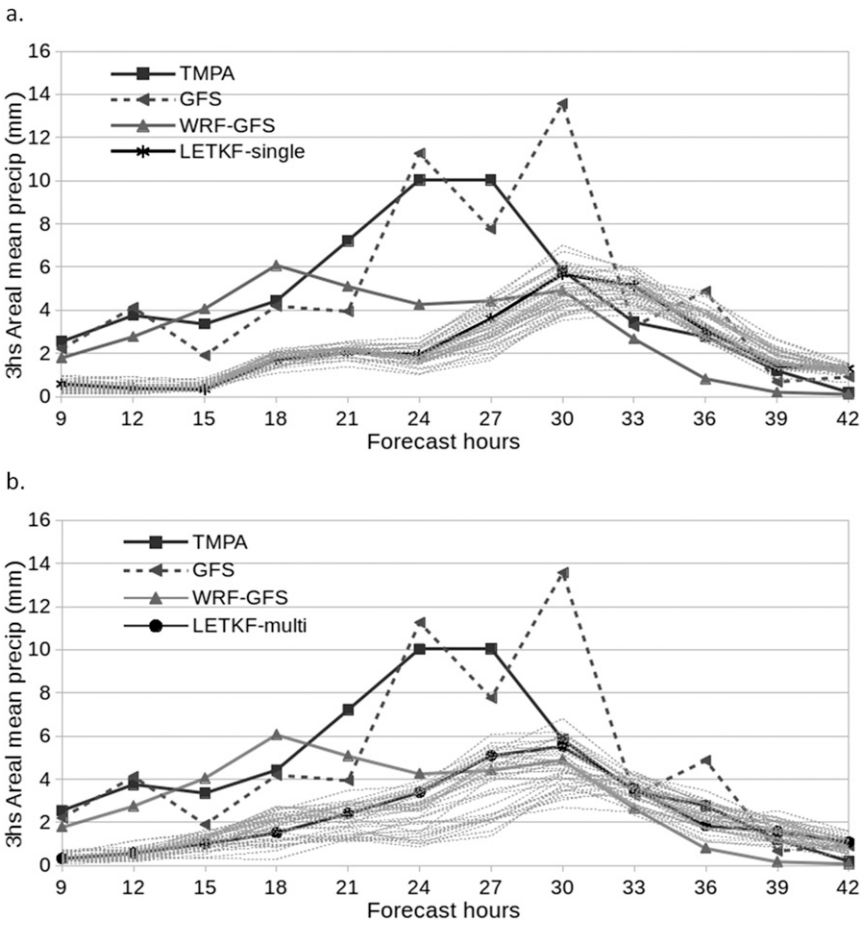

FIG. 11. Spatially averaged precipitation rate [mm $(3\,h)^{-1}$] for the TMPA, GFS, and WRF-GFS forecasts, and the forecasts initialized with the ensemble members and mean of (a) LETKF-single and (b) LETKF-multi for the domain D-36h.

the accumulated precipitation is better captured by the LETKF-multi forecast, particularly if the accuracy of the location of the most intense accumulated precipitation is considered. Moreover, the representation over the Atlantic Ocean in the southeastern part of the domain is also improved in this experiment.

To analyze the overall representation of the time evolution of the MCS by the different forecast experiments, the spatially averaged 3-hourly accumulated precipitation for domain D-36 h presented in Fig. 10a is shown in Fig. 11, including the forecasts of the 40 ensemble members of each experiment (in addition to the runs initialized with the analysis ensemble mean). An important feature is the larger spread of the LETKF-multi members compared to the LETKF-single ones. In this case this is an advantage of the LETKF-multi approach since both ensemble systems are underdispersive, as can be seen from Fig. 11. Overall, the best representation is defined by the GFS, which remains closer to TMPA. The WRF-GFS forecast presents a time evolution, which is similar to the observed; however, the maximum precipitation values between 21- and 27-h lead times are underestimated. Both LETKF-single and LETKF-multi show a lag in the timing of the observed precipitation maximum and an underestimation of precipitation values from the beginning of the forecast and up to 30-h lead time. This underestimation is slightly lower in the forecast initialized from the LETKF-multi analyses. These averages have also been computed for other boxes and in all cases similar conclusions can be drawn from the results (not shown).

To examine the characteristic behavior of each configuration used in the ensemble of LETKF-multi, Fig. 12 shows the average accumulated precipitation forecasted by the multischeme ensemble members that share the same configuration (see Table 1). As expected, each group shows a distinct precipitation pattern; however, those groups sharing the same cumulus scheme are more alike, as could be expected since precipitation rates are strongly related to the cumulus scheme. Particularly, the

groups that share the Grell cumulus parameterization (C, F, and I) displace the system to the north with respect to the TMPA estimate, while the Kain–Fritsch (A, D, and G) and Betts–Miller–Janjic (B, E, and H) groups show a precipitation pattern closer to the estimated precipitation. Moreover, the average forecasts of group B, which uses the YSU PBL scheme, appear to be even closer to the estimation than the LETKF-multi mean forecast. Although this is a specific case study, other studies also suggest that YSU might produce better results in the representation of PBL processes in WRF over southeastern South America (e.g., Ruiz et al. 2010). Hence, with this analysis we want to highlight the importance of taking advantage of the particular members of a multischeme, in addition to the benefits that can be obtained with its ensemble mean.

Quantitative precipitation forecasts are also evaluated using ETS, BIASS, POD, and FAR, over the area D-12h, where the most intense accumulated precipitation was observed (Fig. 10b) in the period between 1800 UTC 6 December and 0600 UTC 7 December. These scores are calculated for precipitation thresholds ranging from 0.5 to 20 mm $(3\,\mathrm{h})^{-1}$ and are shown in Fig. 13. The scores have also been computed for other boxes and periods, and in all cases the same conclusions can be drawn from the results (not shown).

The forecast initialized with the LETKF-multi analysis ensemble mean clearly outperforms the one initialized with the LETKF-single analysis ensemble mean, considering the different scores presented in Fig. 13. In most cases, LETKF-multi is also better than WRF-GFS. These three WRF experiments show an underestimation of the frequency of precipitation, as their values of BIASS are smaller than 1 for almost all the thresholds. This might be related to the dry bias in short-range forecasts produced with WRF over southeastern South America and, particularly, in situations associated with low-level jet events (Ruiz et al. 2010). GFS forecasts outperform all WRF forecasts for almost all the scores and thresholds.

Finally, Fig. 14 shows the 3-hourly precipitation rate PDF computed over the same domain (D-12h) and time frame used for the computation of the scores. The distribution of the GFS is the closest to the distribution of the TMPA. The other three forecasts overestimate the frequency of precipitation rates lower than 10 mm $(3\,\mathrm{h})^{-1}$, while they underestimate the frequency of the most intense rates, which is in agreement with the underestimation observed in Fig. 10. If we compare the two LETKF forecasts, LETKF-multi is closer to the observed distribution than LETKF-single. It is worth noting that for these distributions, specific intervals of precipitation rates are evaluated, while for the BIASS the thresholds indicate precipitation above particular values. Therefore, although an overestimation of the lower rate intervals is detected by looking at the PDFs, this can be compensated with the underestimation of the greater rate intervals observed, leading to the behavior found with BIASS (i.e., underestimation for all thresholds).

Summarizing, the different measures analyzed suggest that the GFS forecast outperforms the three WRF forecasts as expected, since our experiments have coarser resolutions (which is an important feature in the case of an intense convective system). This also suggests that the differences encountered between the GFS and WRF experiments can be explained to a large extent by the model differences, since the WRF Model is always outperformed by the GFS forecast in this case. Results also suggest that an ensemble forecast system initialized from the LETKF-multi analysis outperforms both the one initialized from the LETKF-single analysis and the WRF deterministic forecast initialized from the GFS analysis.

Even though the GFS showed the best scores, the improvement observed in the short-range forecasts and the reasonable representation of the regional atmospheric circulation obtained with LETKF-multi are encouraging. However, a large number of cases should be analyzed in order to obtain robust results. The authors believe that this first development shows the potential of the multischeme DAS to make progress in the implementation of an RNWP system for southern South America.

4. Conclusions

The WRF-LETKF DAS was implemented at SMN, the national weather service of Argentina, during a test period of 2 months using real observations over southern South America. Eight analyses a day were run that could be used for a frequent initialization of short-range ensemble forecasts. The required computational resources to run this DAS are not excessively expensive: an operational implementation is feasible with an 80-core machine and less than a terabyte of disk storage.

In addition, it was found that the performance of the DAS is about 10%–20% worse than the GFS in RMSD for analyzed and 6-h forecasted model variables. As indicated before, we could not expect our 40-km-resolution DAS to outperform the GFS, which at the time of these experiments ran operationally at a higher resolution (27 km) and was able to assimilate satellite radiances from many sensors. However, we showed that the implemented DAS can be complementary to the

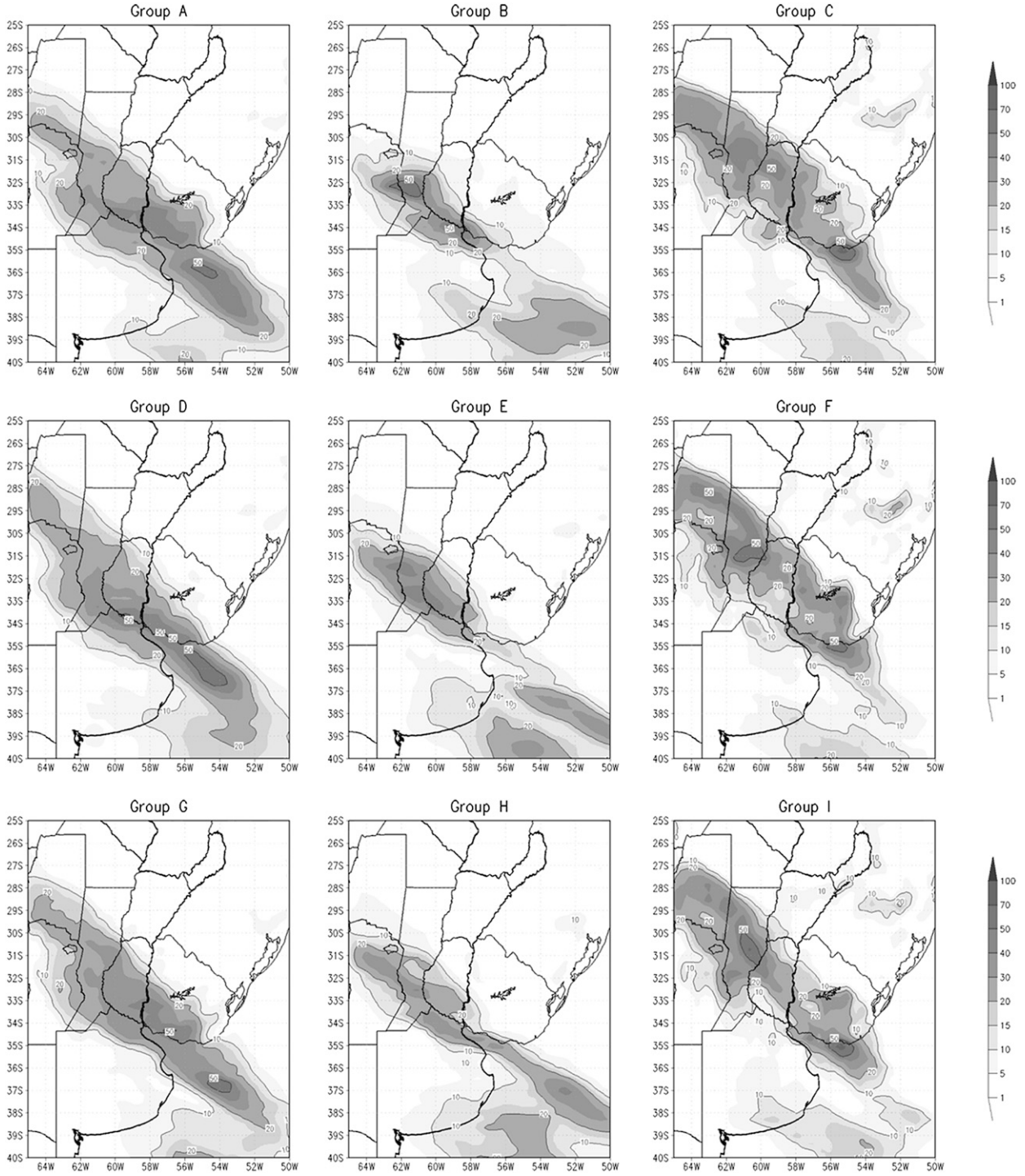

FIG. 12. Mean accumulated precipitation from 1800 UTC 6 Dec to 0600 UTC 7 Dec (mm) for each subgroup of LETKF-multi ensemble members according to Table 1. Contours of 10, 20, and 50 mm are also displayed.

GFS and can be used to generate short-range ensemble forecasts, although many aspects of the precipitation from an MCS in central Argentina were better represented by the GFS.

Overall, LETKF-multi showed better results than LETKF-single, both during the test period and the intense precipitation case study, in accordance with other authors who found good performance in multischeme

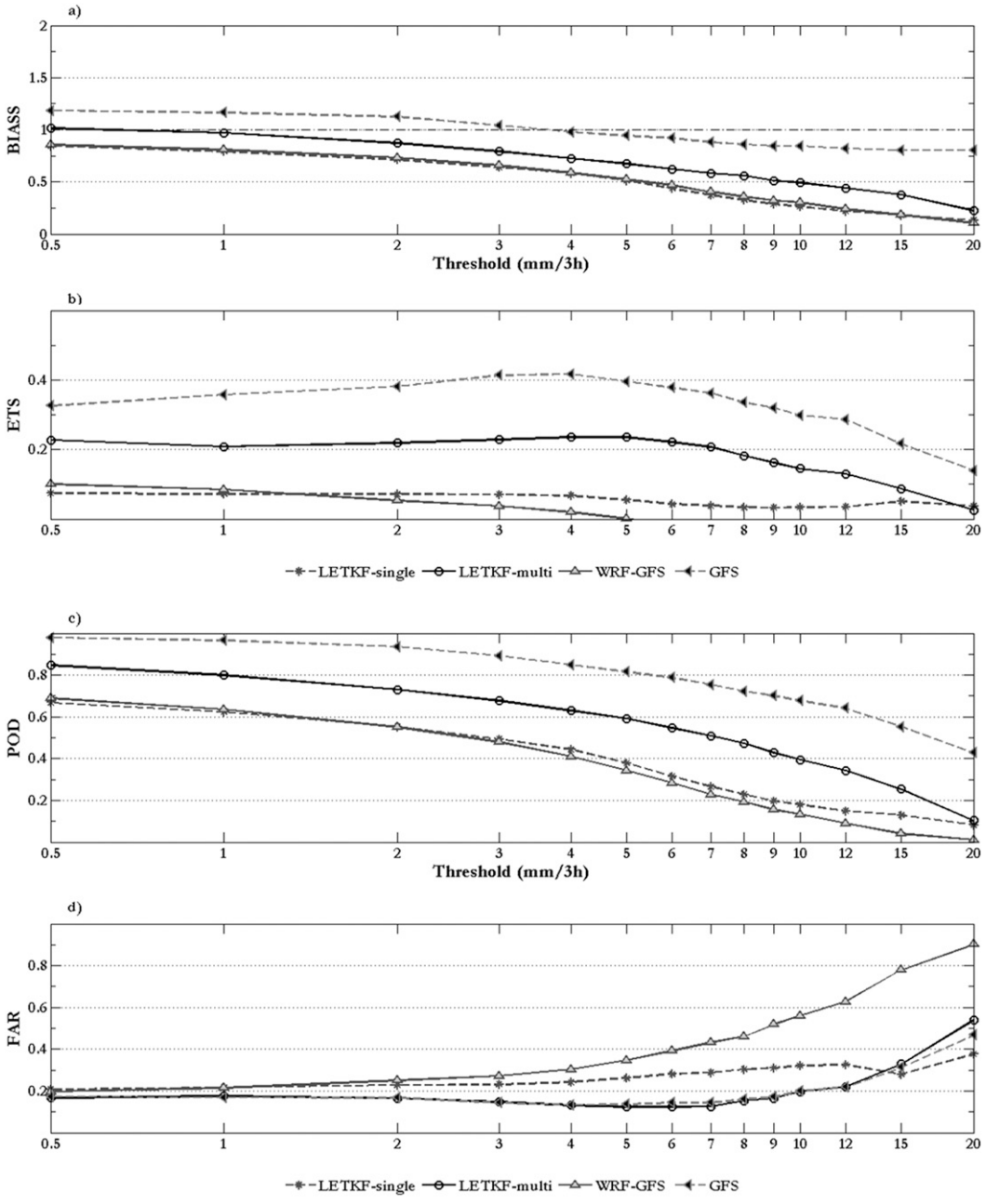

FIG. 13. (a) BIASS, (b) ETS, (c) POD, and (d) FAR computed for the 12-h period from 1800 UTC 6 Dec to 0600 UTC 7 Dec, for the box domain D-12h, for the precipitation forecasts of GFS and WRF-GFS, and the forecasts initialized with the analysis ensemble mean of LETKF-single and LETKF-multi, using the TMPA estimate as the truth.

ensemble systems (Stensrud et al. 2000; Meng and Zhang 2007; Saucedo et al. 2014). Therefore, we consider that the implementation of the LETKF-multi system is preferable with respect to LETKF-single, in order to better represent the model error at no extra computational cost. Nevertheless, a more exhaustive verification should be accomplished, for both the analysis and the forecast over a longer period of time, including situations associated with severe weather over central and northern Argentina. This paper showed the ability to carry out, for the first time in South America, a regional ensemble data assimilation and forecasting system, which has several advantages for a regional NWS. Not only does it provide the basis for a high-resolution

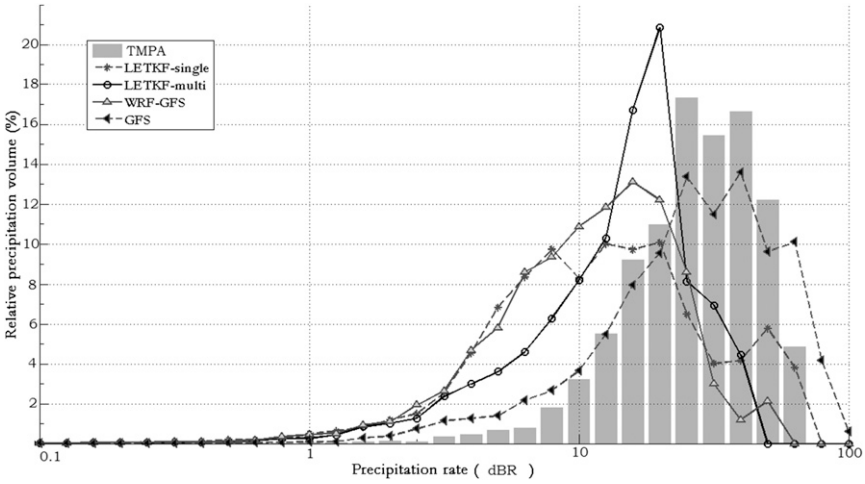

FIG. 14. PDF of 3-hourly precipitation rates computed for the 12-h period from 1800 UTC 6 Dec to 0600 UTC 7 Dec, for the box domain D-12h. Results are for the precipitation forecasts of GFS and WRF-GFS, and for the forecasts initialized with the analysis ensemble mean of LETKF-single and LETKF-multi. The gray bars represent the PDF for the TMPA estimate. Each interval is defined as $\mathrm{dB}R = 10\log\{R/[1\ \mathrm{mm}\ (3\,\mathrm{h})^{-1}]\}$.

multinested system, including ensemble forecasting using regionally available observations such as radar, but it also allows for the development of very high-resolution regional subsystems that could satisfy a country's needs for emergency and/or commercial applications that cannot be simply obtained from the operational GFS, which is already generously made available by the NCEP.

To conclude, we summarize some aspects that will be covered in future work, since this experience has encouraged us to continue developing a WRF-LETKF DAS that can be used operationally at SMN as an RNWP system, to improve regional short-range ensemble forecasts:

- assimilation of AIRS temperature and humidity profiles as in Miyoshi and Kunii (2012) and Jones and Stensrud (2012), in order to compensate for the lack of conventional upper-air observations in our region;
- inclusion of an explicit representation of errors at the domain boundaries in the ensemble generation strategy;
- comparison of the performance of the estimated multiplicative inflation with other ways to improve the estimation of the forecast error covariance matrix, like the options discussed in Whitaker and Hamill (2012) or in Ying and Zhang (2015);
- implementation of the low computational cost smoother proposed by Kalnay and Yang (2010), in order to improve the analysis accuracy; and
- implementation of a hybrid method, like the one proposed by Penny (2014), that combines an ensemble Kalman filter and 3DVAR, which are both already implemented within the WRF Model.

Acknowledgments. The authors are grateful to NCEP who has very generously made available the GFS analyses and forecasts, as well as the PREPBUFR observations. Without this essential information, this work would not have been possible. The authors also thank the National Meteorological Service (SMN) of Argentina, the University of Buenos Aires (UBA), and the Center of Research of the Sea and the Atmosphere (CIMA), for their support of this project. We are grateful to the anonymous reviewers, who enriched this work with their suggestions and comments. The equipment used for this research is supported by PIDDEF 41/2010 and PIDDEF 47/2010. Computations were partially performed at the High Performance Computing System at CIMA supported by the High Performance Computing National System (SNCAD) of Argentina. This work is carried out as part of Grant PIP 11220120100414 CONICET.

REFERENCES

Amitai, E., W. Petersen, X. Llort, and S. Vasiloff, 2011: Multiplatform comparisons of rain intensity for extreme precipitation events. *IEEE Trans. Geosci. Remote Sens.*, **50**, 675–686, doi:10.1109/TGRS.2011.2162737.

Anderson, J. L., and S. L. Anderson, 1999: A Monte Carlo implementation of the nonlinear filtering problem to produce ensemble assimilations and forecasts. *Mon. Wea. Rev.*, **127**, 2741–2758, doi:10.1175/1520-0493(1999)127<2741:AMCIOT>2.0.CO;2.

Azevedo, H., and L. G. de Goncalves, 2015: Observing system experiment in the CPTEC/INPE 3D-Var data assimilation system. *Fourth Int. Symp. on Data Assimilation*, Kobe, Japan,

RIKEN Advanced Institute for Computational Science, P-19. [Available online at http://data-assimilation.jp/isda2015/program/abstract.php?id=P-19.]

Buehner, M., and A. Shlyaeva, 2015: Scale-dependent covariance localization for EnVar data assimilation. *Fourth Int. Symp. on Data Assimilation*, Kobe, Japan, RIKEN Advanced Institute for Computational Science, 8-1. [Available online at http://data-assimilation.jp/isda2015/program/pdf/8-1.pdf.]

Chen, F., and J. Dudhia, 2001: Coupling an advanced land surface–hydrology model with the Penn State–NCAR MM5 modeling system. Part I: Model description and implementation. *Mon. Wea. Rev.*, **129**, 569–585, doi:10.1175/1520-0493(2001)129<0569:CAALSH>2.0.CO;2.

Cressman, G. P., 1959: An operational objective analysis system. *Mon. Wea. Rev.*, **87**, 367–374, doi:10.1175/1520-0493(1959)087<0367:AOOAS>2.0.CO;2.

da Silva, A. M., J. Pfaendtner, J. Guo, M. Sienkiewicz, and S. Cohn, 1995: Assessing the effects of data selection with DAO's Physical-Space Statistical Analysis System. *Proc. Second Int. Symp. on Assimilation of Observation in Meteorology and Oceanography*, Tokyo, Japan, WMO/TD.651.

de Goncalves, L. G., and H. Azevedo, 2015: Study of the impact of satellite data, radiosondes and GPS in a SACZ episode using G3DVar. *Fourth Int. Symp. on Data Assimilation*, Kobe, Japan, RIKEN Advanced Institute for Computational Science, P-20. [Available online at http://data-assimilation.jp/isda2015/program/abstract.php?id=P-20.]

Dillon, M. E., Y. Garcia Skabar, and M. Nicolini, 2013: Desempeño del pronóstico de modelos de alta resolución, en un área limitada: Análisis de la estación de verano 2010–2011. *Meteorológica*, **38**, 69–89.

Du, J., G. DiMego, B. Zhou, D. Jovic, B. Ferrier, B. Yang, and S. Benjamin, 2014: NCEP regional ensembles: Evolving toward hourly-updated convection-allowing scale and storm-scale predictions within a unified regional modeling system. *Proc. 22nd Conf. on Numerical Weather Prediction/26th Conf. on Weather Analysis and Forecasting*, Atlanta, GA, Amer. Meteor. Soc., J1.4. [Available online at https://ams.confex.com/ams/94Annual/webprogram/Paper239030.html.]

Dudhia, J., 1989: Numerical study of convection observed during the Winter Monsoon Experiment using a mesoscale two-dimensional model. *J. Atmos. Sci.*, **46**, 3077–3107, doi:10.1175/1520-0469(1989)046<3077:NSOCOD>2.0.CO;2.

Gandin, L. S., 1963: *Objective Analysis of Meteorological Fields* (in Russian). Hydrometeoizdat, 242 pp.

García Skabar, Y., and M. Nicolini, 2009: Enriched analyses with assimilation of SALLJEX data. *J. Appl. Meteor. Climatol.*, **48**, 2425–2440, doi:10.1175/2009JAMC2091.1.

Grell, G. A., and D. Devenyi, 2002: A generalized approach to parameterizing convection combining ensemble and data assimilation techniques. *Geophys. Res. Lett.*, **29**, 1693, doi:10.1029/2002GL015311.

Hamrud, M., M. Bonavita, and L. Isaksen, 2014: EnKF and hybrid gain ensemble data assimilation. ECMWF Tech. Memo. 733, 36 pp.

Herdies, D. L., S. H. Ferreira, J. P. Bonatti, R. Cintra, and A. da Silva, 2002: O sistema de assimilaçao de dados atmosféricos global do CPTEC/INPE. *XII Congresso Brasileiro de Meteorologia*, Foz de Iguaçu, Brazil, Sociedade Brasileira de Meteorologia, 4028–4033.

——, J. A. Aravéquia, S. H. Ferreira, R. V. Andreoli, L. F. Sapucci, and J. G. Z. Mattos, 2007: Assimilaçao de dados no CPTEC/INPE (Data assimilation in CPTEC/INPE). 12 pp. [Available online at assimila.cptec.inpe.br/~rassmla/pubs/pub_r09.pdf.]

Hong, S.-Y., and J.-O. J. Lim, 2006: The WRF single-moment 6-class microphysics scheme (WSM6). *J. Korean Meteor. Soc.*, **42**, 129–151.

——, Y. Noh, and J. Dudhia, 2006: A new vertical diffusion package with an explicit treatment of entrainment processes. *Mon. Wea. Rev.*, **134**, 2318–2341, doi:10.1175/MWR3199.1.

Houtekamer, P. L., L. Lefaivre, J. Derome, H. Ritchie, and H. L. Mitchell, 1996: A system simulation approach to ensemble prediction. *Mon. Wea. Rev.*, **124**, 1225–1242, doi:10.1175/1520-0493(1996)124<1225:ASSATE>2.0.CO;2.

——, X. Deng, H. L. Mitchell, S. J. Baek, and N. Gagnon, 2014: Higher resolution in an operational ensemble Kalman filter. *Mon. Wea. Rev.*, **142**, 1143–1162, doi:10.1175/MWR-D-13-00138.1.

Huffman, G. J., and D. T. Bolvin, 2013: TRMM and other data precipitation data set documentation. NASA Goddard Space Flight Center, 42 pp. [Available online at ftp://precip.gsfc.nasa.gov/pub/trmmdocs/3B42_3B43_doc.pdf.]

——, and Coauthors, 2007: The TRMM Multisatellite Precipitation Analysis (TMPA): Quasi-global, multiyear, combined-sensor precipitation estimates at fine scales. *J. Hydrometeor.*, **8**, 38–55, doi:10.1175/JHM560.1.

Hunt, B. R., E. J. Kostelich, and I. Szunyogh, 2007: Efficient data assimilation for spatiotemporal chaos: A local ensemble transform Kalman filter. *Physica D*, **230**, 112–126, doi:10.1016/j.physd.2006.11.008.

Janjic, Z. I., 1994: The step-mountain eta coordinate model: Further developments of the convection, viscous sublayer, and turbulence closure schemes. *Mon. Wea. Rev.*, **122**, 927–945, doi:10.1175/1520-0493(1994)122<0927:TSMECM>2.0.CO;2.

——, 2002: Nonsingular implementation of the Mellor–Yamada level 2.5 scheme in the NCEP Meso Model. NCEP Office Note 437, 61 pp.

Jones, T. A., and D. J. Stensrud, 2012: Assimilating AIRS temperature and mixing ratio profiles using an ensemble Kalman filter approach for convective-scale forecasts. *Wea. Forecasting*, **27**, 541–564, doi:10.1175/WAF-D-11-00090.1.

Kain, J. S., 2004: The Kain–Fritsch convective parameterization: An update. *J. Appl. Meteor.*, **43**, 170–181, doi:10.1175/1520-0450(2004)043<0170:TKCPAU>2.0.CO;2.

Kalnay, E., 2003: *Atmospheric Modeling, Data Assimilation and Predictability.* Cambridge University Press, 341 pp.

——, and S.-C. Yang, 2010: Accelerating the spin-up of ensemble Kalman filtering. *Quart. J. Roy. Meteor. Soc.*, **136**, 1644–1651, doi:10.1002/qj.652.

——, H. Li, T. Miyoshi, S.-C. Yang, and J. Ballabrera-Poy, 2007: 4D-Var or ensemble Kalman filter? *Tellus*, **59A**, 758–773, doi:10.1111/j.1600-0870.2007.00261.x.

Keyser, D., 2013: PREPBUFR processing at NCEP. NOAA/NWS/NCEP/EMC. [Available online at http://www.emc.ncep.noaa.gov/mmb/data_processing/prepbufr.doc/document.htm.]

Kleist, D. T., 2012: An evaluation of hybrid variational–ensemble data assimilation for the NCEP GFS. Ph.D. thesis, University of Maryland, College Park, 149 pp.

Köpken, C., G. Kelly, and J.-N. Thépaut, 2004: Assimilation of Meteosat radiance data within the 4D-Var system at ECMWF:

Assimilation experiments and forecast impact. *Quart. J. Roy. Meteor. Soc.*, **130**, 2277–2292, doi:10.1256/qj.02.230.

Lorenc, A. C., 2003: Modelling of error covariances by four-dimensional variational data assimilation. *Quart. J. Roy. Meteor. Soc.*, **129**, 3167–3182, doi:10.1256/qj.02.131.

Machado, L., and Coauthors, 2013: The CHUVA field campaign: Overview. *CHUVA Int. Workshop*, San Pablo, Brazil, Satellite Division and Environmental Systems/CPTEC. [Available online at http://chuvaproject.cptec.inpe.br/portal/workshop/materials.html.]

McCarty, W., G. Jedlovec, T. L. Miller, 2009: Impact of the assimilation of Atmospheric Infrared Sounder radiance measurements on short-term weather forecasts. *J. Geophys. Res.*, **114**, D18122, doi:10.1029/2008JD011626.

Meng, Z., and F. Zhang, 2007: Tests of an ensemble Kalman filter for mesoscale and regional-scale data assimilation. Part II: Imperfect model experiments. *Mon. Wea. Rev.*, **135**, 1403–1423, doi:10.1175/MWR3352.1.

Michalakes, J., J. Dudhia, D. Gill, T. Henderson, J. Klemp, W. Skamarock, and W. Wang, 2004: The Weather Research and Forecast Model: Software architecture and performance. *Proc. 11th ECMWF Workshop on the Use of High Performance Computing in Meteorology*, Reading, United Kingdom, ECMWF, 156–168.

Miyoshi, T., 2011: The Gaussian approach to adaptive covariance inflation and its implementation with the local ensemble transform Kalman filter. *Mon. Wea. Rev.*, **139**, 1519–1535, doi:10.1175/2010MWR3570.1.

——, and M. Kunii, 2011: The local ensemble transform Kalman filter with the Weather Research and Forecasting Model: Experiments with real observations. *Pure Appl. Geophys.*, **169**, 321–333, doi:10.1007/s00024-011-0373-4.

——, and ——, 2012: Using AIRS retrievals in the WRF-LETKF system to improve regional numerical weather prediction. *Tellus*, **64A**, 18408, doi:10.3402/tellusa.v64i0.18408.

——, S. Yamane, and T. Enomoto, 2007: Localizing the error covariance by physical distances within a local ensemble transform Kalman filter (LETKF). *SOLA*, **3**, 89–92, doi:10.2151/sola.2007-023.

——, Y. Sato, and T. Kadowaki, 2010: Ensemble Kalman filter and 4D-Var intercomparison with the Japanese Operational Global Analysis and Prediction System. *Mon. Wea. Rev.*, **138**, 2846–2866, doi:10.1175/2010MWR3209.1.

Mlawer, E. J., S. J. Taubman, P. D. Brown, M. J. Iacono, and S. A. Clough, 1997: Radiative transfer for inhomogeneous atmosphere: RRTM, a validated correlated-*k* model for the longwave. *J. Geophys. Res.*, **102**, 16 663–16 682, doi:10.1029/97JD00237.

Ota, Y., J. C. Derber, E. Kalnay, and T. Miyoshi, 2013: Ensemble-based observation impact estimates using the NCEP GFS. *Tellus*, **65A**, 20038, doi:10.3402/tellusa.v65i0.20038.

Pauley, P., N. Baker, R. Langland, L. Xu, D. Merkova, R. Gelaro, and C. Velden, 2012: The impact of satellite atmospheric motion vectors in the U.S. Navy Global Data Assimilation System—The superob procedure. *Extended Abstracts*, *11th Int. Winds Workshop*, Auckland, New Zealand, EUMETSAT. [Available online at http://www.eumetsat.int/website/wcm/idc/idcplg?IdcService=GET_FILE&dDocName=PDF_CONF_P60_S4_10_PAULEY_V&RevisionSelectionMethod=LatestReleased&Rendition=Web.]

Penny, S. G., 2014: The hybrid local ensemble transform Kalman filter. *Mon. Wea. Rev.*, **142**, 2139–2149, doi:10.1175/MWR-D-13-00131.1.

Ruiz, J. J., C. Saulo, and J. Nogués-Paegle, 2010: WRF Model sensitivity to choice of parameterization over South America: Validation against surface variables. *Mon. Wea. Rev.*, **138**, 3342–3355, doi:10.1175/2010MWR3358.1.

Saito, K., H. Seko, M. Kunii, and T. Miyoshi, 2012: Effect of lateral boundary perturbations on the breeding method and the local ensemble transform Kalman filter for mesoscale ensemble prediction. *Tellus*, **64A**, 11594, doi:10.3402/tellusa.v64i0.11594.

Salio, P., M. Nicolini, and E. J. Zipser, 2007: Mesoscale convective systems over southeastern South America and their relationship with the South American low-level jet. *Mon. Wea. Rev.*, **135**, 1290–1309, doi:10.1175/MWR3305.1.

——, M. P. Hobouchian, Y. Garcia Skabar, and D. Vila, 2014: Evaluation of high-resolution satellite precipitation estimates over southern South America using a dense rain gauge network. *Atmos. Res.*, **163**, 146–161, doi:10.1016/j.atmosres.2014.11.017.

Saucedo, M., J. Ruiz, and C. Saulo, 2014: Sensitivity experiments to design a regional assimilation system combining the LETKF and the WRF Model. *Abstracts*, *The World Weather Open Science Conf.*, Montreal, QC, Canada, WMO–ICSU–Environment Canada, SCI-POS1038. [Available online at http://wwosc2014.org/pdf/20140825-WWOSC-FinalBookofAbstracts.pdf.]

Saulo, C., S. Cardazzo, J. Ruiz, C. Campetella, A. Rolla, 2008: El sistema de pronóstico experimental del Centro de Investigaciones del Mar y la Atmósfera. *Meteorologica*, **33**, 83–97.

Schwartz, C. S., Z. Liu, Y. Chen, and X.-Y. Huang, 2012: Impact of assimilating microwave radiances with a limited-area ensemble data assimilation system on forecasts of Typhoon Morakot. *Wea. Forecasting*, **27**, 424–437, doi:10.1175/WAF-D-11-00033.1.

Seko, H., T. Miyoshi, Y. Shoji, and K. Saito, 2011: Data assimilation experiments of precipitable water vapour using the LETKF system: intense rainfall event over Japan 28 July 2008. *Tellus*, **63A**, 402–414, doi:10.1111/j.1600-0870.2010.00508.x.

Skamarock, W., and Coauthors, 2008: A description of the Advanced Research WRF version 3. NCAR Tech. Note TN–468+STR, 113 pp., doi:10.5065/D68S4MVH.

Stensrud, D. J., J.-W. Bao, and T. T. Warner, 2000: Using initial condition and model physics perturbations in short-range ensemble simulations of mesoscale convective systems. *Mon. Wea. Rev.*, **128**, 2077–2107, doi:10.1175/1520-0493(2000)128<2077:UICAMP>2.0.CO;2.

Sukoriansky, S., B. Galperin, and V. Perov, 2005: Application of a new spectral model of stratified turbulence to the atmospheric boundary layer over sea ice. *Bound.-Layer Meteor.*, **117**, 231–257, doi:10.1007/s10546-004-6848-4.

Vera, C., and Coauthors, 2006: The South American Low-Level Jet Experiment. *Bull. Amer. Meteor. Soc.*, **87**, 63–77, doi:10.1175/BAMS-87-1-63.

Verspeek, J. A., A. Stoffelen, M. Portabella, H. Bonekamp, C. Anderson, and J. Figa, 2009: Validation and calibration of ASCAT using CMOD5.n. *IEEE Trans. Geosci. Remote Sens.*, **48**, 386–395, doi:10.1109/TGRS.2009.2027896.

Wang, X., D. Barker, C. Snyder, and T. Hamill, 2008: A hybrid ETKF–3DVAR data assimilation scheme for the WRF Model. Part I: Observing system simulation experiment. *Mon. Wea. Rev.*, **136**, 5116–5131, doi:10.1175/2008MWR2444.1.

Wang, Y., S. Tascu, F. Weidle, and K. Schmeisser, 2012: Evaluation of the added value of regional ensemble forecasts on global ensemble forecasts. *Wea. Forecasting*, **27**, 972–987, doi:10.1175/WAF-D-11-00102.1.

Warner, T. T., R. A. Peterson, and R. E. Treadon, 1997: A tutorial on lateral boundary conditions as a basic and potentially serious limitation to regional numerical weather prediction. *Bull. Amer. Meteor. Soc.*, **78**, 2599–2617, doi:10.1175/1520-0477(1997)078<2599:ATOLBC>2.0.CO;2.

Whitaker, J. S., and T. M. Hamill, 2012: Evaluating methods to account for system errors in ensemble data assimilation. *Mon. Wea. Rev.*, **140**, 3078–3089, doi:10.1175/MWR-D-11-00276.1.

Xu, D., Z. Liu, X.-Y. Huang, J. Min, and H. Wang, 2013: Impact of assimilating IASI radiance observations on forecasts of two tropical cyclones. *Meteor. Atmos. Phys.*, **122**, 1–18, doi:10.1007/s00703-013-0276-2.

Yang, S.-C., E. Kalnay, B. Hunt, and N. E. Bowler, 2009: Weight interpolation for efficient data assimilation with the local ensemble transform Kalman filter. *Quart. J. Roy. Meteor. Soc.*, **135**, 251–262, doi:10.1002/qj.353.

Ying, Y., and F. Zhang, 2015: An adaptive covariance relaxation method for ensemble data assimilation. *Quart. J. Roy. Meteor. Soc.*, **141**, 2898–2906, doi:10.1002/qj.2576.

Zhang, F., C. Snyder, and J. Sun, 2004: Impacts of initial estimate and observation availability on convective-scale data assimilation with an ensemble Kalman filter. *Mon. Wea. Rev.*, **132**, 1238–1253, doi:10.1175/1520-0493(2004)132<1238:IOIEAO>2.0.CO;2.